Nanomed. J. 8(1): 30-41, Winter 2021

RESEARCH PAPER

Analysis of physical dose enhancement in nano-scale for nanoparticle-based radiation therapy: a Cluster and endothelial cell model

Elham Mansouri [1], Asghar Mesbahi [2, 3*], Parivar Yazdani [2]

[1]Drug Applied Research Center, Tabriz University of Medical Sciences, Tabriz, Iran
[2]Molecular Medicine Research center, Tabriz University of Medical Sciences, Tabriz, Iran
[3]Medical Radiation Sciences Research Team, Tabriz University of Medical Sciences, Tabriz, Iran

ABSTRACT

Objective(s): One major difficulty of conventional radiotherapy is the lack of selectivity between the tumor and the organs at risk. In nanoparticle aided radiotherapy, heavy elements are present at higher concentrations in the tumor than normal tissues. This study aimed to model the characteristics of secondary electrons generated from the interaction of clusters comprised of five different nanoparticles including Gold, Gadolinium, Iridium, Bismuth, and Hafnium atoms with low energy x-rays (similar to brachytherapy sources in terms of energy) as a function of nanoparticle size and beam energy.

Materials and Methods: To better evaluate the contributions of secondary electrons in energy deposition, and also to develop a framework in analyzing further measurements in the future, we attempted to enhance and promote existing mathematical models for energy deposition in endothelial cells by nanoparticle-enhanced radiotherapy. Also, the MCNPX Monte Carlo code was used to model the identical geometry and the dose enhancement factor was calculated for all types of simulated nano-clusters.

Results: Our results showed that for our model consist of a nano-cluster and an endothelial cell the DEF significantly depends on the energy of photons and L- and K-edge binding energy of the atoms inside the nano-cluster. However, for Gd at the energy 60 keV, a higher dose enhancement factor was seen.

Conclusion: It can be concluded that the mathematical model considers the DEF variation with photon energy and the effect of NP type is considered in DEF calculations. However, the MC method has indicated very high sensitivity to photon energy, and NP type compared to the mathematical method.

Keywords: *Dose Enhancement, Radiation Therapy, Radiosensitization, Nanoparticle; Nano-Cluster*

How to cite this article

Mansouri E, Mesbahi A, Yazdani P. Analysis of physical dose enhancement in nano-scale for nanoparticle-based radiation therapy: a Cluster and endothelial cell model. Nanomed J. 2021; 8(1): 30-41. DOI: 10.22038/nmj.2021.08.04

INTRODUCTION

The growth of nanotechnology and its biomedical applications (e.g., biosensing, therapeutic applications, medical imaging, radiation therapy, and targeted gene and drug delivery) have fueled by the chemical design and synthesis of novel nanoparticles [1-18]. Exploiting nanoparticles as potent radiosensitizers is currently receiving enormous attention since radiation therapy of cancers by X-rays relies on the energy deposition within a tumor mediated by secondary electrons. This happens via various physical interactions between photons and tumor tissue cells which lead to direct and indirect (free radical production) damages of DNA. Tumor cell kill is related to the double-strand break of the DNA in the cell nucleus [19]. Nanoparticles can be distributed inside tumors and be tumor-selective by labeling with ligands or molecules [20]. Indeed, the underlying principle of nanoparticle localized radio-enhancement has been a higher energy deposition in the vicinity of the DNA or other cellular components such as mitochondria by secondary electrons emitted from the irradiated nanoparticle. NPs could amplify radiation-induced biological damage of cancer cells or their vasculature and thus provides the possibility of improved radiotherapeutic index [21].

To improve the normal-tissue sparing and deliver higher doses to tumor volume, adding heavy nanoparticles (High-Z material) to the

* *Corresponding Author Email: amesbahi2010@gmail.com*
Note. This manuscript was submitted on July 1, 2020; approved on October 13, 2020

tumor has been extensively presented in the literature focusing on the nanoparticle size, shape, concentration, surface coating, and distribution [22-27]. According to the recent studies, kilovoltage photon beams produced significantly 2 or 3 times more interactions with the heavy-elements-NPs compared to the megavoltage beam [28, 29]. Note that, application of heavy-element-NPs as radiosensitizers with low-energy X or gamma-ray irradiations could produce an effective dose enhancement in radiation dose delivery and cause drastically increased radiobiological damages [30-32]. Physically, range and linear energy transfer (LET) of escaping photoelectric products (primary and secondary photoelectrons, Auger electrons, Coster-Kronig electrons, fluorescent X-rays, and other short-range electrons) released from the irradiated nanoparticle are the important factors that impact energy deposition in tumor cell and its damage. These produced secondary electrons are responsible for additional energy deposition in the presence of heavy-elements-NPs. The size of NPs used for radiosensitization affects how they interact with the biological system as well as radiation. For small NPs, meager photon interactions in the NP volume occur but the resulting secondary electrons mostly escape from the nanoparticle surface and reach the tumor. While large NPs suffer from the lack of escaped secondary electrons but more photon interaction is possible for them [33].

There are myriad Monte Carlo (MC) and analytical studies on the estimation of physical dose enhancement of NPs in radiation therapy [34-37]. However, their estimations show a wide range of dose enhancement factor (DEF) for different material types and photon energies. Among these studies, some of them have tried to model the DEF of NPs by using mathematical methods. Mathematical modeling of radiation interaction with NPs has been an essential part of theoretical studies in radiation biology and physics. However, most of the developed mathematical models in this regard are simplified, abstract, and incomplete, and do not provide efficient interpretations or predictions of physical phenomena concerning radiation interaction with. For example, one of the first analytical studies on dose enhancement characterization in nano-scale and at cell level introduced a geometry [32] which was followed by further theoretical studies that attempted to calculate the delivered dose to an endothelial cell in the presence of NPs [38, 39]. In these models, the contribution of Auger electrons and florescent X-rays in the dose enhancement was not considered. In this regard, a comparative study was carried out which indicated a considerable discrepancy between analytical and MC results and led to the conclusion that the MC method is a better approach to evaluate delivered dose enhancement [40]. Another MC-based computational study was addressed the problem by in-silico-in Vitro estimations of radio-enhancement for a cluster of gold NPs [41]. In practice, NPs are almost found clustered together in cell cytoplasm which is larger than individual NPs and is very different from the studied scenarios where a single nanosphere is irradiated by photons[42]. Although, there is a disconnection between the theoretically predicted DEF and experimentally observed results, a complete and precise physical estimation could resolve the existing discrepancies. Consequently, it is beneficial to design a mathematical model that considers all physical aspects including primary and secondary photoelectron, Auger electrons, and x-ray fluorescent in energy deposition around NPs and incorporates all produced secondary electrons energy in a physical model for NP-based radiation therapy.

This study aimed to model the dose deposition in an endothelial cell by secondary electrons generated from the interaction of a cluster of NPs with low energy photons of 29, 60, and 100 keV.

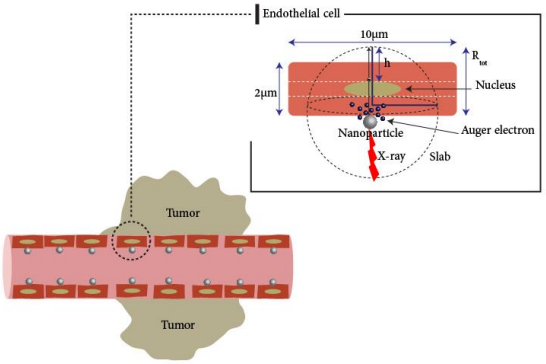

Fig 1. Schematic representation of tumor and its vasculature. A single endothelial cell and a nano-cluster was modeled in both analytical and Monte Carlo methods

To better evaluate the contributions of secondary electrons in energy deposition, and also to develop a framework in analyzing further measurements in the future, we attempted to

enhance and promote the existing mathematical model for energy deposition in endothelial cells by NP-enhanced radiotherapy. To evaluate the effect of the element type in dose deposition inside the cell, five different nano-clusters composed of Gold, Gadolinium, Iridium, Bismuth, and Hafnium NPs were modeled. Also, the MCNPX MC code was used to model the identical geometry, and DEFs were calculated for all simulated nano-clusters. The results of the developed model were compared with the MC results.

METHODS

Mathematical modeling

The geometry of the model was depicted in Fig 1. As can be seen, a slab of the tumor vascular endothelial cell has been modeled with dimensions of 2 µm (thickness) × 10 µm (length) × 10 µm (width) and a single cluster of Gold, Gd, Ir, Bi, and Hf NPs with the size of 400 nm (to avoid intracellular transmission) was simulated attached to the outer surface of it. The contribution of a cluster of NPs in increasing radiotherapy efficiency is measured by the dose enhancement factor

$$\mathrm{DEF} = \frac{\mathrm{D_W + D_{cluster}}}{\mathrm{D_W}} \quad (1)$$

DW is the dose delivered to the endothelial cell when the nano-cluster is not present and Dcluster is delivered dose to the endothelial cell by the nano-cluster.

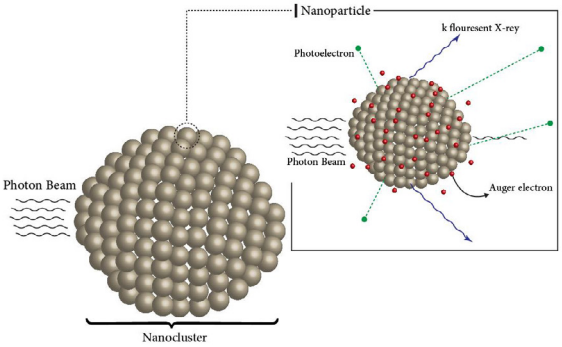

Fig 2. Interaction of low energy photons (KeV) with a heavy element-nano-cluster. When a heavy element-nano-cluster is irradiated by low energy photon, secondary electrons are generated as byproduct of photoelectric interaction. If the energy of the incident photon is less than K-edge binding energy of the targeted NP, photoelectrons release from the L and M shells. Afterward, the vacancy is filled by an electron from the upper shell and then an Auger electron or cascade of Auger electrons is ejected and followed by emission of cascade of low energy X-rays. In addition, when incident photon's energy exceeds the K-shell binding energy of the targeted NP, the photoelectrons are ejected from K-shell. Afterward, the vacancy is filled by an electron from the upper shell and then a K-florescent X-ray is emitted. In the following, an Auger electron or cascade of Auger electrons and cascade of florescent X-rays are produced

Also, (Dcluster+ DW) is the dose delivered to the endothelial cell in the presence of a nano-cluster. A nano-cluster undergoes a photoelectric interaction when low energy photons incident to it. Fig 2 shows the byproducts of a low energy photon beam interaction with a nano-cluster.

Dose delivered to the cytoplasm from photoelectrons

Each photoelectron emitted from a cluster of Gold, Gd, Ir, Bi, and Hf NPs will deposit their energy locally as a function of its initial kinetic energy. This kinetic energy can be found by subtracting the target-edge (K, L, or M shells) electron binding energy from the energy of the incident photon. The closer is the energy of an incident photon to the binding energy of the collided shell, the larger is the probability for photoelectric interaction. Over 80% of all photoelectric interactions occur with K-shell electrons when incident photon's energy exceeds the K-shell binding energy [43]. However, for the energies lower than the K-shell binding energy, the L-shell is the most probable source of photoelectrons generation. The total number of produced photoelectrons and Auger electrons from each nano-cluster is related to the photon flux and density and size of the nano-cluster.

We used the approach of Ngwa et al, [44] to calculate the DEF arising from photoelectrons (DEFPE) by the following equation:

$$\mathrm{DEF_{PE}} = \frac{\mathrm{D_W + D_{cluster(PE)}}}{\mathrm{D_W}} \quad (2)$$

$$\mathrm{D_W} = \Sigma_E \Phi E \left(\frac{\mu_{en}}{\rho}\right)_E \quad (3)$$

Where Φ is photon flux (photon/cm2), E is energy of incident photon (Joule), and (µen/ρ) is (cm2/g) at a given energy E.

The number of photons incident to the cluster (N0) was calculated by the following equation

$$N_0 = \Phi \times \pi r^2 \quad (4)$$

Where r is the radius of the cluster.

The number of photoelectric interactions (NPE) happens in collided nanoparticle could be derived by this equation:

$$N_{PE} = N_0 - N = N_0\left(1 - e^{(-\frac{\mu_{PE}}{\rho})_E \rho_{NP}(\frac{4r}{3})}\right) \sim N_0 \frac{4}{3}\left(\frac{\mu_{en}}{\rho}\right)_E \times \rho_{cluster} \times r \quad (5)$$

Where N is the number of photons passes the NP without interaction is the cross-section of photoelectric interaction in an atom (cm2/g), ρNP is density (g/cm2) of the NP.

The number of clusters attached to the cell is:

$$N_{cluster} = \frac{C\rho_{EC}V_{EC}}{\frac{4}{3}\pi r^3 \rho_{NP}} \quad (6)$$

Where C, V_{EC}, and ρEC are the concentration, volume, and density of cell

The total number of produced photoelectrons for the number of clusters attached to the cell was calculated by:

$$N_{PEtotal} = N_{cluster} \times N_{PE} \quad (7)$$

The dose delivered to the cell by the irradiated cluster is:

$$D_{cluster} = \frac{E_C \times N_{PEtotal}}{V_{EC} \times \rho_{EC}} \quad (8)$$

EC is the energy deposited in the endothelial cell by the photoelectrons [38]:

$$E_C = \frac{1}{R_{total}} \int_r^{R_{total}} (3.16(R_{total} - x)^{-0.435} + 0.005(R_{total} - x)^{0.33}) \quad (9)$$

The total range of photoelectrons in the endothelial cell is calculated by:

$$Rtotal = 0.0431(E - E_{edge} + 0.367)^{1.679} - 0.007 \quad (10)$$

1/Rtotal is the fraction of the endothelial cell area in which the produced photoelectron could deposit their energy in.

Eedge is the binding energy of an electron that photon incident to it. As shown in Fig2, photoelectrons could reach out of the endothelial cell (Rtotal) and could not deposit their energy completely in the cell. Therefore, the following equations were used:

$$D_{cluster} = \frac{1}{R_{total}} C\Phi \left(\frac{\mu_{PE}}{\rho}\right)_E \int_r^{R_{total}} (3.16(R_{total} - x + 0.007)^{-0.435} + 0.005(R_{total} - x)^{0.33}) \quad (11)$$

$$DEF_{PE} = \frac{1}{R_{total}} \frac{C}{E_{Ph}} \left(\frac{\mu_{PE}/\rho}{\mu_{en}/\rho}\right)_E \int_r^{R_{total}} (3.16(R_{total} - x)^{-0.435} + 0.005(R_{total} - x)^{0.33}) \quad (12)$$

The Auger effect is a physical phenomenon in which the filling of an inner-shell vacancy of an atom is accompanied by the emission of an electron from the same atom. Electrons produced through the Auger effect are referred to as Auger electrons, Coster-Kronig electrons (CK), and super Coster-Kronig (SCK) electrons. For the NPs employed in our study, super Coster-Kronig electrons production was impossible (due to very close energy levels of electrons in M- and L-subshells) and only Coster-Kronig and Auger electrons could be generated from M shell as byproducts of the Auger effect. For our studied high-z atoms of Au, Bi, Gd, Hf, and Ir, the probability of Auger electron production is the highest (~1) if the energy of the incident photon is lower than K-shell binding energy and the photoelectron exits from the L-shell. While the fluorescent x-ray emission probability is very low (~zero) [45]. For each photoelectron release from the L-shell of irradiated NP, one Auger electron (with the energy of 3-10 keV for applied NPs) or a cascade of Auger electrons (with the energy of about 1.20-4 keV for applied NPs) or a CK electron (with energy less than 2 keV) could be produced from the M-shell followed by a cascade of secondary fluorescent X-rays (mostly with energy less than 1 keV) emission. These energy ranges are derived by consideration of each subshell binding energy and possible transitions. The energy of produced Auger and CK electrons depends on the atomic structure of irradiated material and clearly on the energy difference between the shell with the vacancy and the energy level of the shell in which the electron falls into the vacancy. The energy and production probability of CK electrons is very low and is ignorable. Derived from equation 8, the total range of Auger electrons (with energy less than 10 keV and with an average energy of 4keV) in water is 0.591μm. Therefore, they deposit their energy completely in the endothelial cell. Besides, the probability of the Auger electron production is the lowest (~zero) and the fluorescent X-ray emission probability is the highest (~1) if the photoelectron exits from the K-shell (when the energy of the incident photon is higher than the K-shell binding energy) [45]. For each primary photoelectron (with energy less than 20 keV for applied NPs) released from the K-shell of irradiated NP, a florescent X-ray (Kα or Kβ) is emitted. Kα and Kβ characteristic x-rays are generated when the K–shell electrons are replaced with an electron from the L- and M-shell respectively. It should be noted here that the electron transitions from M1 and L1 levels to the K-shell are forbidden transitions according to quantum mechanics laws. The K-florescent X-ray energy can be found by subtracting K-edge binding energy from the energy of the L- or M-shells. Following fluorescent X-ray emission, one or a cascade of Auger electrons (L-MM) with energy less than 10 keV and cascade of low energy X-rays are generated.

The number of Auger electrons (NAug) ejected from each nano-cluster is relative to the photoelectron production probability and the number of incident photons:

$$N_{Aug} = N_{ph} \times P_{PE} \quad (13)$$

For simplicity, we assumed that photoelectron

production is followed by ejection of one Auger electron (with the energy of 3-10 KeV) instead of the Auger cascade with more than one Auger electron with energy less than 2keV.
Also, the total number of Auger electrons was derived by:

$$N_{Augtotal} = N_{cluster} \times N_{Aug} \quad (14)$$

If the average energy of Auger electrons assumed 4keV then Rtotal of Auger electrons is 0.591µm then the DEFAug was derived by:

$$DEF_{Aug} = 1 + \frac{c}{E_{Ph}} \left(\frac{\mu_{PE}/\rho}{\mu_{en}/\rho}\right)_E (3.136) \quad (15)$$

DEFtotal both for the energies higher and lower than the K shell binding energy of targeted NP could be derived by:

$$DEF_{total} = DEF_{PE} + DEF_{Aug} \quad (16)$$

Auger electrons deposit their energy in the vicinity of the NP and near the membrane of the endothelial cell. Auger electrons have a great contribution to energy deposition because of their high LET. The M shell is the source of the most produced Auger electrons.

Dose delivered to the endothelial cell's nucleus from photoelectrons

Only photoelectrons could be considered for DEF calculation of the nucleus because Auger electrons don't have enough energy to reach the nucleus of the endothelial cell. The nucleus is considered to be located at the center of the endothelial cell with a diameter of 0.5 µm and a thickness of 1.0 µm. It was calculated by the following equations:

$$DEF_{PE} = 1 + \frac{1}{2R_{total}} \frac{C}{E_{Ph}} \left(\frac{\mu_{PE}/\rho}{\mu_{en}/\rho}\right)_E \int_r^{R_{total}} (3.16(R_{total} - x)^{-0.435} + 0.005(R_{total} - x)^{0.33}) \quad (17)$$

$$DEF_{total} = DEF_{PE} \quad (18)$$

To determine the accuracy of the model presented above, MC simulation was carried out and its predictions were compared to the above mentioned mathematical model. In this regard, MC–generated photons with the energy of 29, 60, and 100 keV were used for the calculation and the number of attached clusters were considered to be the same as in the mathematical model (=1). The equation 19 calculated the DEF for one nano-cluster attached to an endothelial cell.

$$DEF_{PE} = \frac{2}{3} \frac{tr^3}{R_{total}} \frac{1}{E_P} \frac{\rho_{NP}}{V_{EC} \times \rho_{EC}} \left(\frac{\mu_{PE}/\rho}{\mu_{en}/\rho}\right)_E \int_r^{R_{total}} (3.16(R_{total} - x + 0.007)^{-0.435} + 0.005(R_{total} - x)^{0.33}) \quad (19)$$

MC simulations for DEF estimations

In the current study, we used the MCNPX (2.7.0) MC code for our simulations. The simulated geometry is seen in Fig 2. A cluster of spherical NPs composed of 512 spheres was simulated and it was modeled like a cluster attached to the cell membrane of an endothelial cell. It resembles a cluster in the proximity of a tumor cell which was separated from it by an endothelial cell of a vessel. The diameter of the nano-cluster was considered 400 nm.

The dose delivered by secondary electrons was calculated in the cytoplasm and nucleus of the endothelial cell using *F8: e tally which scores energy deposition in terms of MeV per initial photon.

The energy deposited in the cell cytoplasm and nucleus was converted to Gy by multiplying MeV by 1.6 ×10-13 and dividing by mass of cytoplasm and nucleus. DEF for each energy and nanoparticle was calculated using equation 1.

MC simulations for secondary electrons spectra calculation

To accurately estimate the contribution of Auger electrons and other secondary electrons in DEF calculations, we obtained the energy spectra of produced secondary electrons by the MC method. For scoring energy spectra we used F2: e tally which calculates the number of electrons crossing a surface of an NP.

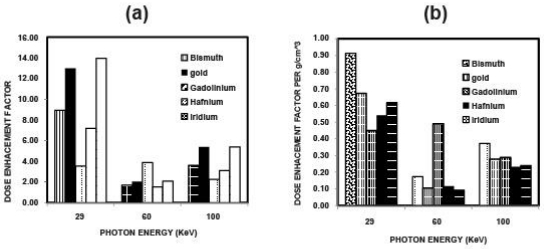

Fig 3. a) cellular DEF as a function of energy of photon for 400nm of Au, Bi, Gd, Ir, and Hf nano-clusters. b) cellular DEF/ density as a function of energy of photon for Gold, Bi, Gd, Ir, and Hf nano-clusters of 400nm

RESULTS AND DISCUSSION

The ultimate goal of using NPs in radiation therapy is to enhance ionizing energy deposition from nanometer to micrometer range at a tumor cell.

One major difficulty of conventional radiotherapy is the lack of selectivity between the tumor and the organs at risk [46].

Table 1. Dose enhancement factor values in the endothelial cell when irradiated to 29, 60, and 100 keV photons for different concentrations

NP	Photon energy (kev)	DEF_{PE}		DEF_{Aug}		DEF_{total}	
		7mg/g	20mg/g	7mg/g	20mg/g	7mg/g	20mg/g
Au	29	1.11	1.33	1.12	1.36	2.23	2.69
	60	1.02	1.05	1.05	1.146	2.07	2.196
	100	1.05	1.15	1.074	1.22	2.12	2.37
Bi	29	1.10	1.28	1.12	1.34	2.38	2.46
	60	1.017	1.049	1.045	1.13	2.066	2.17
	100	1.03	1.10	1.052	1.16	2.08	2.26
Gd	29	1.04	1.12	1.06	1.18	2.10	2.30
	60	1.14	1.41	1.12	1.36	2.26	2.77
	100	1.14	1.41	1.12	1.36	2.26	2.77
Ir	29	1.08	1.24	1.06	1.18	2.14	2.42
	60	1.015	1.041	1.04	1.118	2.055	2.159
	100	1.015	1.041	1.04	1.118	2.055	2.159
Hf	29	1.06	1.19	1.09	1.26	2.14	2.41
	60	1.01	1.03	1.03	1.09	2.04	2.12
	100	1.016	1.045	1.054	1.1	2.06	2.14

In nanoparticle-aided radiotherapy, heavy elements are present at higher concentrations in the tumor than normal tissues. On the other hand, they have significantly higher mass-energy absorption coefficient (μen/ ρ) and photoelectric cross-sections relative to normal tissue. NP-based radiation therapy could increase tumor control probability and decrease normal tissue complication probability (NTCP). Also, low energy photons have a large cross-section of photoelectric interaction on the K- and L-shell of heavy elements [47].

Thus, most researchers have employed heavy-element-NPs as radiosensitizers to increase photoelectric photon absorption of tumor cells at kilovoltage photon energies [48-50].

To interpret our data, we have considered two different scenarios for DEF calculation. In the first scenario, the incident photon energy is lower than the K-shell binding energy of applied NPs. The produced photoelectrons deposit most of their energy out of the targeted cell because of their long-range. While the Auger electrons have higher LET and deposit their energy in the vicinity of the NP and completely inside the simulated cell. In the second scenario, the incident photon energy is higher than the K-shell binding energy of applied NPs. In this case, most of the incident photon's energy is carried by K-florescent X-ray, and produced photoelectrons have energy less than 20 keV.

The effects of varying the nanoparticle concentration on the dose enhancement are considered in this study. Table 1 shows the results from the mathematical model, where the variation of cellular DEF due to photoelectrons and Auger electrons as a function of NP concentration for 400nm of Gold, Bi, Gd, Ir, and Hf nano-clusters are presented when irradiated to 29, 60 and 100 keV photons. According to the results, the increased nano-cluster concentration leads to an increase in DEF which was in good agreement with Roeske et al. and Hossain et al. [32, 38]. Also, for the energies of 29 and 100 keV and, gold-nano-cluster has the highest DEF (cytoplasm and nucleus) among the other materials which are close to DEF in presence of Bi-nano-cluster. While for the 60keV photon, the highest DEF value was found for Gd. The photoelectric interaction is the most likely to occur if the energy of the incident photon is closer to the binding energy of the electron which it interacts with. Also, the probability of photoelectric interaction decreases with an increase in photon's energy.

According to results shown in table 1, the DEF value for the energies of 29 and 100 keV is higher than for 60 keV (except for Gd), since the energy of incident 29 and 100 keV photon is closer to the L and K-shell's binding energy of gold, Bi, Hf, and Ir, respectively. For Gd, the K-shell binging energy is 50.24 keV and is much closer to the energy of the 60kev photon.

Therefore, the DEF value for Gd-nano-cluster is the highest for 60 keV photon interaction. As shown in Fig 3.a which resulted from MC calculations, for the energy of 29 and 100KeV, and the model of one nan-cluster attached to an endothelial cell, Iridium has the highest DEF value among the other applied NPs and its value is close to that of Au-NP. The reason is that for the similar

size of the nano-cluster the number of Ir atoms per a nano-cluster is the highest because of the high density of the Ir. However, for the energy of 60 KeV which is close to the K-shell binding energy of Gd, the highest DEF value is for Gd-NP. Besides, when the effect of density of the nano-cluster is not considered, for the energy of 29 and 100 KeV, Bi-NP has the highest DEF value and the lowest value is for the Ir-NP(see Fig 3.b).

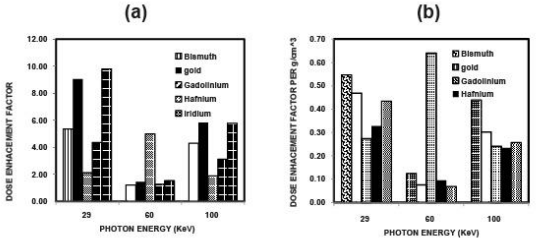

Fig 4. a) DEF of the nucleus as a function of energy of photon for 400nm of Au, Bi, Gd, Ir, and Hf nano-clusters. b) DEF/density of the nucleus as a function of energy of photon for Gold, Bi, Gd, Ir, and Hf nano-clusters of 400nm

Table 2. Dose enhancement factor values in the nucleus of endothelial cell when irradiated to 29, 60, and 100 keV photon for different concentrations

NP	Photon energy (kev)	DEF_{PE}	
		7mg/g	20mg/g
Au	29	1.05	1.16
	60	1.02	1.025
	100	1.025	1.07
Bi	29	1.05	1.14
	60	1.08	1.024
	100	1.01	1.05
Gd	29	1.02	1.06
	60	1.07	1.20
	100	1.004	1.012
Ir	29	1.04	1.12
	60	1.007	1.020
	100	1.012	1.034
Hf	29	1.034	1.098
	60	1.005	1.01
	100	1.008	1.022

The similar results were calculated for the nucleus of an endothelial cell which is presented in Fig 4.a and b.

Auger electrons are not engaged in dose enhancement of the nucleus of the cell because of their short range.

Table 2 shows the variation of DEF induced in the nucleus of an endothelial cell due to photoelectrons as a function of NP concentration for 400nm of Gold, Bi, Gd, Ir, and Hf nano-clusters when irradiated to 29, 60, and 100 keV photons.

Figs 5,6 and 7 presented the spectrum of secondary electrons generated from an (Au, Bi, Ir, Hf, and Gd) nano-clusters (400nm) irradiated by 29, 60, and 100 KeV photons.

For the energies of 29 and 60 KeV, two peaks are corresponding to the photoelectrons generated from L and M shells and Auger electrons and cascade of Auger electrons are presented. Additionally, for the Gd- nano-clusters irradiated to 60 KeV photons and for all of the studied nano-clusters irradiated to 100 KeV photons, three peaks corresponding to the photoelectrons generated from K, L, and M shells, secondary photoelectrons and Auger electrons and cascade of Auger electrons are presented. The Auger electrons could have the energy up to 10 keV for the applied NPs.

The photoelectrons could be attenuated by the nano-cluster and leave the nano-cluster with lower energy.

The other low energy electrons which are seen in the electron spectra could be attenuated photoelectrons. In the presented mathematical model, the attenuation of the secondary electrons by the NP is not considered.

Table 3. Dose enhancement factor values in the endothelial cell when irradiated to 29, 60, and 100 keV photons for one nano-cluster attached to endothelial cell

NP	Photon energy (kev)	Mathematical red\sult			MC result
		DEF_{PE}	DEF_{Aug}	DEF_{total}	DEF
Au	29	1.05	1.14	2.19	8.93
	60	1.008	1.0428	2.05	1.68
	100	1.0165	1.0465	2.062	3.63
Bi	29	1.03	1.075	2.10	12.98
	60	1.0048	1.025	2.03	2.03
	100	1.0123	1.022	2.034	5.38
Gd	29	1.01	1.03	2.04	3.54
	60	1.027	1.0488	2.08	3.87
	100	1.0017	1.01	2.01	2.26
Ir	29	1.058	1.147	2.20	13.95
	60	1.0083	1.045	2.053	2.09
	100	1.0131	1.043	2.056	5.40
Hf	29	1.027	1.074	2.10	7.18
	60	1.0039	1.028	2.033	1.53
	100	1.0051	1.0219	2.027	3.09

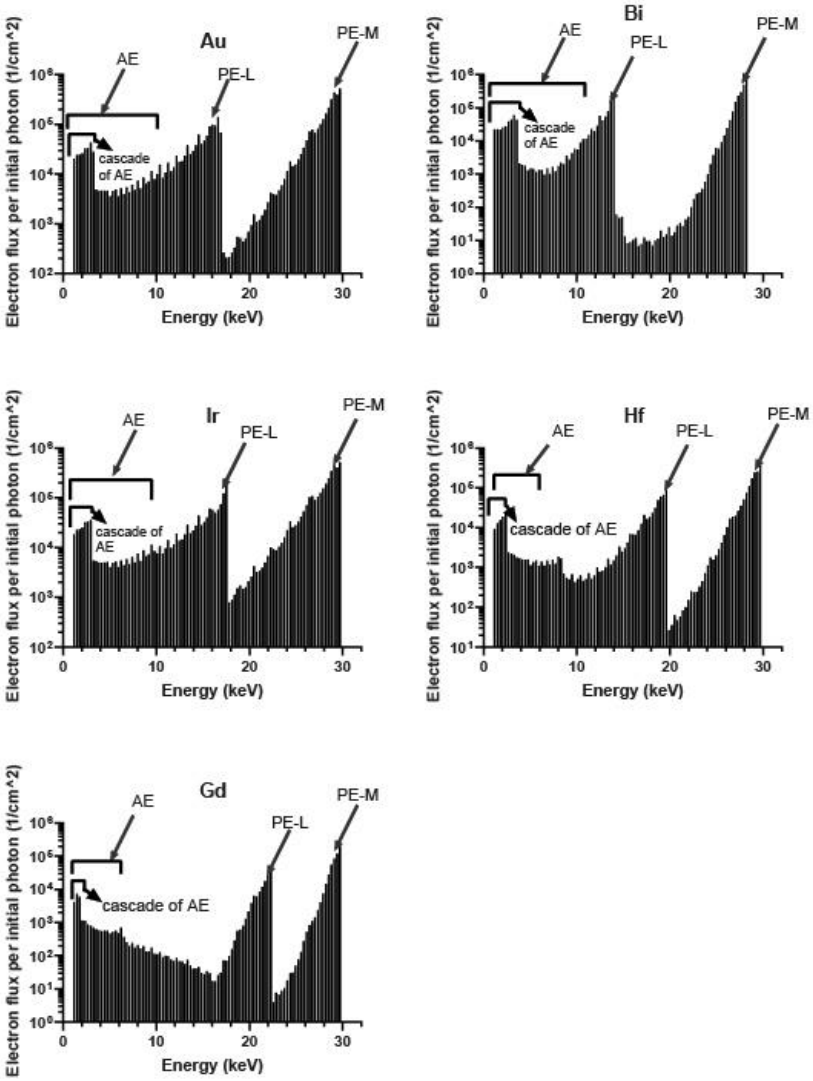

Fig 5. spectrum of secondary electrons generated from a nano-cluster (400nm) irradiated with 29KeV KeV photons. Auger Electrons (AEs), Photo Electrons (PEs) are presented. PE-L and PE-M are corresponding to photoelectrons released from K, L and M shells respectively

Table 4. Dose enhancement factor values in the nucleus of endothelial cell when irradiated to 29, 60, and 100 keV photon for one nano-cluster attached to endothelial cell

	Photon energy (kev)	Mathematical model DEF_{PE}	MC
Au	29	1.029	9.04
	60	1.004	1.45
	100	1.0083	5.83
Bi	29	1.016	5.35
	60	1.0024	1.21
	100	1.0013	4.29
Gd	29	1.005	2.13
	60	1.0137	4.99
	100	1.0008	1.88
Ir	29	1.0291	9.79
	60	1.0042	1.53
	100	1.0065	5.78
Hf	29	1.0136	4.36
	60	1.0020	1.26
	100	1.0025	3.11

Thus, our proposed model can be optimized by taking into account the self-absorption and attenuation effect of NP or clusters.

For the photon with the energy higher than K-shell binding energy, the photoelectron production is followed by a K-florescent X-ray emission which carries the majority of the incident photon's energy.

On the other hand, the produced K-florescent X-ray has a mean free path about 100µm and it is less probable to deposit its energy in the targeted endothelial cell.

Therefore, most of the energy of the primary photon is deposited far from the targeted endothelial cell.

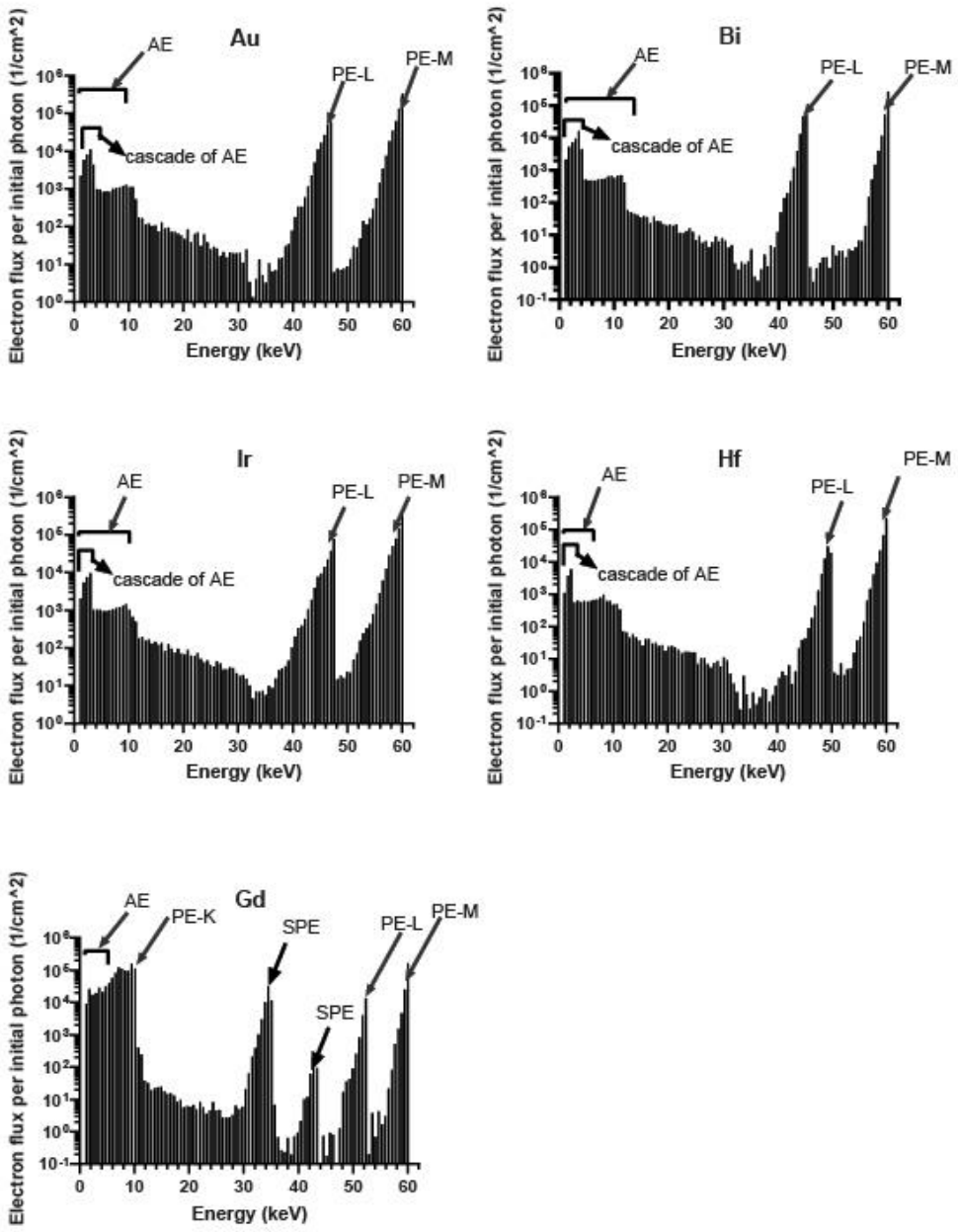

Fig 6. spectrum of secondary electrons generated from a nano-cluster (400nm) irradiated with 60KeV photons. Auger Electrons (AEs), Photo Electrons (PEs) and Secondary Photo Electrons (SPEs) are presented. PE-K, PE-L and PE-M are corresponding to photoelectrons released from K, L and M shells respectively

The data of DEF values for the model of one nano-cluster attached to the endothelial cell and the nucleus resulted from mathematical and MC Modellings is presented in table 3 and table 4 respectively.

There is a good agreement between MC and mathematical model results for the energy of 60 keV Fig 8.b.

While, for the energies of 100 and 29 keV which are close to the binding energy of k- and L-shells of applied heavy elements, a significant difference between MC and mathematical model results is seen (Fig 8.a and c). It seems that some physical phenomena are missed in our mathematical model when the energy of an incident photon is close to the binding energy of K- and L- shell.

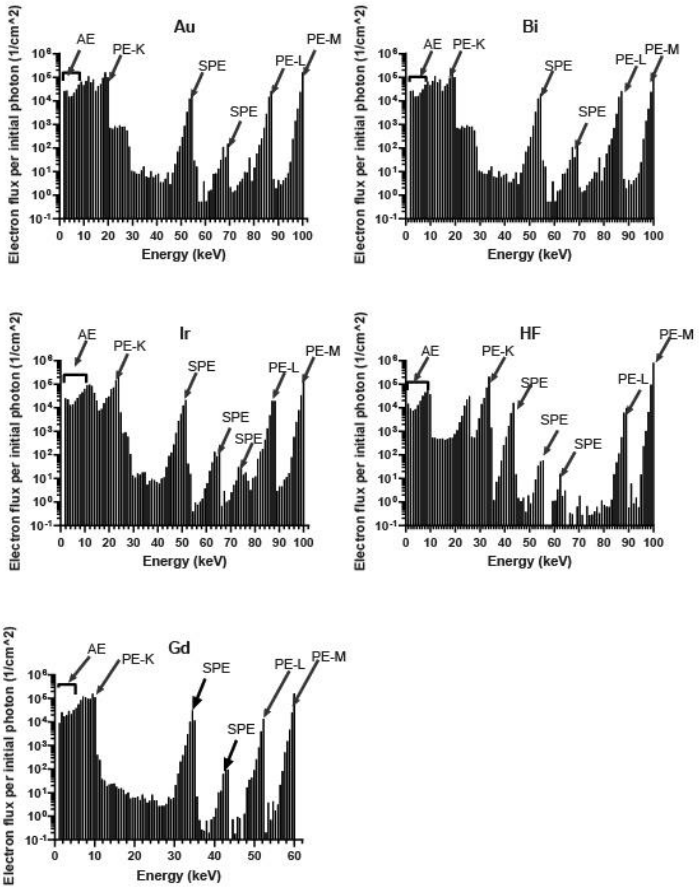

Fig 7. spectrum of secondary electrons generated from a nano-cluster (400nm) irradiated with 100 KeV photons. Auger Electrons (AEs), Photo Electrons (PEs) and Secondary Photo Electrons (SPEs) are presented. PE-K, PE-L and PE-M are corresponding to photoelectrons released from K, L and M shells respectively

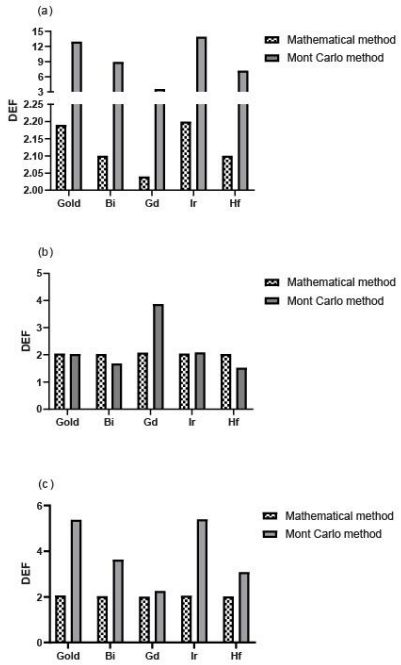

Fig 8. DEF values resulted from MC and mathematical calculations

However, it should be mentioned here that this mathematical model can be used primarily for comparing different NPs in the enhancement of dose delivered to the targeted endothelial cell but there were significant differences in the calculated DEF between mathematical and MC methods in 29 and 100 keV.

CONCLUSION

Our results showed that for our model consist of a nano-cluster and an endothelial cell the DEF significantly depends on the energy of photons and L- and K-edge binding energy of the atoms inside the nano-cluster. For the energy of 29 and 100 KeV, the mathematical model which calculated DEF for 7 and 20 mg/g of nano-clusters indicated that Au and Bi had the highest DEF among studied NPs. Besides, Gd, Hf, and Ir had very close DEF for 29 and 100 keV photons.

However, at the energy of 60 keV, the highest DEF value was for Gd. Our MC model which was performed for one nano-cluster and did not take

into account the concentration of NPs, showed comparable DEFs for Ir and Au and Bi while the highest DEF was Ir-nano-cluster. MC method calculated very high DEF up to 14 for NPs while the mathematical model was not able to follow the MC calculated values and its maximum value was 2.2 for Ir.

It can be concluded that the mathematical model considers the DEF variation with photon energy and the effect of NP type is considered in DEF calculations. However, the MC method has indicated very high sensitivity to photon energy, and NP type compared to the mathematical method.

The application of Ir-NPs as new radiosensitizers is recommended. Also, the conduction of experimental methods for DEF estimation of different NPs is suggested.

ACKNOWLEDGMENTS

This project was supported by Drug Applied research center of Tabriz Univerity Of Medical Science as a part of the PhD thesis in medical physics. The authors would like to thank the molecular medicine research center and medical physics department of Tabriz Univerity Of Medical Science for providing the required computer hardware for MC simulation.

REFERENCES

1.Yazdani P, Mansouri E, Eyvazi S, Yousefi V, Kahroba H, Hejazi MS. Layered double hydroxide nanoparticles as an appealing nanoparticle in gene/plasmid and drug delivery system in C2C12 myoblast cells. Artif Cells Nanomed Biotechnol. . 2019; 47(1): 436-442.

2.Mansouri E, Tarhriz V, Yousefi V, Dilmaghani A. Intercalation and release of an anti-inflammatory drug into designed three-dimensionally layered double hydroxide nanostructure via calcination–reconstruction route. Adsorption. 2020.

3.Ghavami SM, Ghiasi H, Mesbahi A. Monte Carlo modeling of the yttrium-90 nanospheres application in the liver radionuclide therapy and organs doses calculation. Nucl Technol Radiat Prot. 2016; 31(1): 89-96.

4.Mesbahi A, Famouri F, Ahar MJ, Ghaffari MO, Ghavami SM. A study on the imaging characteristics of Gold nanoparticles as a contrast agent in X-ray computed tomography. PJMPE. 2017; 23(1): 9-14.

5.Pirayesh Islamian J, Hatamian M, Aval NA, Rashidi MR, Mesbahi A, Mohammadzadeh M. Targeted superparamagnetic nanoparticles coated with 2-deoxy-D-gloucose and doxorubicin more sensitize breast cancer cells to ionizing radiation. Breast. 2017;33: 97-103.

6.Mesbahi A, Ghiasi H. Shielding properties of the ordinary concrete loaded with micro- and nano-particles against neutron and gamma radiations. Appl Radiat Isot. 2018; 136: 27-31.

7.Verdipoor K, Alemi A, Mesbahi A. Photon mass attenuation coefficients of a silicon resin loaded with WO3, PbO, and Bi2O3 Micro and Nano-particles for radiation shielding. Radiat Phys Chem. 2018; 147: 85-90.

8.Badrigilan S, Shaabani B, Gharehaghaji N, Mesbahi A. Iron oxide/bismuth oxide nanocomposites coated by graphene quantum dots: "Three-in-one" theranostic agents for simultaneous CT/MR imaging-guided in vitro photothermal therapy. Photodiagnosis Photodyn Ther. 2019; 25: 504-514.

9.Jangjoo AG, Ghiasi H, Mesbahi A. A Monte Carlo study on the radio-sensitization effect of gold nanoparticles in brachytherapy of prostate by 103Pd seeds. PJMPE. 2019; 25(2): 87-92.

10.Khodadadi A, Nedaie HA, Sadeghi M, Ghassemi MR, Mesbahi A, Banaee N. Determination of the dose enhancement exclusively in tumor tissue due to the presence of GNPs. Appl Radiat Isot. 2019; 145: 39-46.

11.Malekzadeh R, Mehnati P, Sooteh MY, Mesbahi A. Influence of the size of nano- and microparticles and photon energy on mass attenuation coefficients of bismuth–silicon shields in diagnostic radiology. Radiol Phys Technol. 2019; 12(3): 325-334.

12.Mesbahi A, Verdipoor K, Zolfagharpour F, Alemi A. Investigation of fast neutron shielding properties of new polyurethane-based composites loaded with B4C, BeO, WO3, ZnO, and Gd2O3 micro-and nanoparticles. Pjmpe. 2019; 25(4): 211-219.

13.Zareei L, Divband B, Mesbahi A, Khatamian M, Kiani A, Gharehaghaji N. A new potential contrast agent for magnetic resonance imaging: Iron Oxide-4A nanocomposite. JBPE. 2019; 9(2): 211-216.

14.Afkham Y, Mesbahi A, Alemi A, Zolfagharpour F, Jabbari N. Design and fabrication of a Nano-based neutron shield for fast neutrons from medical linear accelerators in radiation therapy. Radiat Oncol. 2020; 15(1).

15.Badrigilan S, Shaabani B, Aghaji NG, Mesbahi A. Graphene Quantum Dots-Coated Bismuth Nanoparticles for Improved CT Imaging and Photothermal Performance. Int J Nanosci. 2020; 19(1).

16.Mortezazadeh T, Gholibegloo E, Khoobi M, Alam NR, Haghgoo S, Mesbahi A. In vitro and in vivo characteristics of doxorubicin-loaded cyclodextrine-based polyester modified gadolinium oxide nanoparticles: a versatile targeted theranostic system for tumour chemotherapy and molecular resonance imaging. J Drug Target. 2020; 28(5): 533-546.

17.Sadeghian M, Akhlaghi P, Mesbahi A. Investigation of imaging properties of novel contrast agents based on gold, silver and bismuth nanoparticles in spectral computed tomography using Monte Carlo simulation. PJMPE. 2020; 26(1): 21-29.

18.Verdipoor K, Mesbahi A. Radiation shielding features of ordinary and high-density concretes loaded with PbO micro and nanoparticles against high-energy photons. IJMP. 2020; 17(3): 205-212.

19.Butterworth K, Wyer JA, Fournet M, Latimer C, Shah M, Currell F. Variation of Strand Break Yield for Plasmid DNA Irradiated with High-Z Metal Nanoparticles. Radiat Res. 2008; 170: 381-387.

20.Bazak R, Houri M, El Achy S, Kamel S, Refaat T. Cancer active targeting by nanoparticles: a comprehensive review of literature. J Cancer Res Clin Oncol. 2015; 141(5): 769-

784.
21.Zheng Y, Sanche L. Gold nanoparticles enhance DNA damage induced by anti-cancer drugs and radiation. Radiation research. 2009;172(1):114-9.
22.Cooper DR, Bekah D, Nadeau JL. Gold nanoparticles and their alternatives for radiation therapy enhancement. Front Chem. 2014; 2(86).
23.Jain S, Hirst DG, O'Sullivan JM. Gold nanoparticles as novel agents for cancer therapy. Br J Radiol. 2012; 85(1010): 101-113.
24.Vallières S. Dose Enhancement with Nanoparticles in Radiotherapy Using Gold-Doxorubicin Conjugates 2016.
25.Berbeco RI, Ngwa W, Makrigiorgos GM. Localized dose enhancement to tumor blood vessel endothelial cells via megavoltage X-rays and targeted gold nanoparticles: new potential for external beam radiotherapy. Int J Radiat Oncol. 2011; 81: 270.
26.Hainfeld JF, Dilmanian FA, Slatkin DN, Smilowitz HM. Radiotherapy enhancement with gold nanoparticles. J Pharm Pharmacol. 2008; 60: 977.
27.Hildenbrand G, Metzler P, Pilarczyk G, Bobu V, Kriz W, Hosser H. Dose enhancement effects of gold nanoparticles specifically targeting RNA in breast cancer cells. PLoS One. 2018; 13(1): e0190183-e.
28.Leung MK, Chow JC, Chithrani BD, Lee MJ, Oms B, Jaffray DA. Irradiation of gold nanoparticles by x-rays: Monte Carlo simulation of dose enhancements and the spatial properties of the secondary electrons production. Med Phys. 2011; 38(2): 624-631.
29.Mesbahi A, Jamali F, Gharehaghaji N. Effect of Photon Beam Energy, Gold Nanoparticle Size and Concentration on the Dose Enhancement in Radiation Therapy. BioImpacts : BI. 2013; 3: 29-35.
30.Kobayashi K, Usami N, Porcel E, Lacombe S, Le Sech C. Enhancement of radiation effect by heavy elements. Mutat Res. 2010; 704: 123.
31.Butterworth KT, McMahon SJ, Currell FJ, Prise KM. Physical basis and biological mechanisms of gold nanoparticle radiosensitization. Nanoscale. 2012; 4(16): 4830-4838.
32.Roeske JC, Nunez L, Hoggarth M, Labay E, Weichselbaum RR. Characterization of the theorectical radiation dose enhancement from nanoparticles. Technol Cancer Res Treat. 2007; 6(5): 395-401.
33.Zygmanski P, Sajo E. Nanoscale radiation transport and clinical beam modeling for gold nanoparticle dose enhanced radiotherapy (GNPT) using X-rays. Br J Radiol. 2016; 89(1059): 20150200.
34.Ghasemi Jangjoo A, Ghiasi H, Mesbahi A. A Monte Carlo study on the radio-sensitization effect of gold nanoparticles in brachytherapy of prostate by 103Pd seeds. PJMPE. 2019; 25: 87-92.
35.Khodadadi A, Nedaie HA, Sadeghi M, Ghassemi MR, Mesbahi A, Banaee N. Determination of the dose enhancement exclusively in tumor tissue due to the presence of GNPs. Appl Radiat Isot. 2019; 145: 39-46.
36.Mesbahi A. A review on gold nanoparticles radiosensitization effect in radiation therapy of cancer. Rep Pract Oncol Radiother. 2010; 15(6): 176-180.
37.Mesbahi A, Jamali F, Garehaghaji N. Effect of photon beam energy, gold nanoparticle size and concentration on the dose enhancement in radiation therapy. Bioimpacts. 2013; 3(1): 29-35.
38.Hossain M, Su M. Nanoparticle Location and Material-Dependent Dose Enhancement in X-ray Radiation Therapy. J Phys Chem C. 2012; 116(43): 23047-23052.
39.Lee C, Cheng NN, Davidson RA, Guo T. Geometry Enhancement of Nanoscale Energy Deposition by X-rays. J Phys Chem C. 2012; 116(20): 11292-11297.
40.Paro AD, Hossain M, Webster TJ, Su M. Monte Carlo and analytic simulations in nanoparticle-enhanced radiation therapy. Int J Nanomedicine . 2016; 11: 4735-4741.
41.Retif P, Reinhard A, Héna P, Jouan-Hureaux V, Chateau A, Sancey L. Monte Carlo simulations guided by imaging to predict the in vitro ranking of radiosensitizing nanoparticles. Int J Nanosci. 2016;Volume 11.
42.Villagomez-Bernabe B, Currell FJ. Physical Radiation Enhancement Effects Around Clinically Relevant Clusters of Nanoagents in Biological Systems. Sci Rep. 2019; 9(1): 8156-.
43.McMahon SJ, Hyland WB, Muir MF, Coulter JA, Jain S, Butterworth KT. Biological consequences of nanoscale energy deposition near irradiated heavy atom nanoparticles. Sci Rep. 2011; 1.
44.Ngwa W, Makrigiorgos GM, Berbeco RI. Applying gold nanoparticles as tumor-vascular disrupting agents during brachytherapy: estimation of endothelial dose enhancement. Phys Med Biol. 2010; 55: 6533.
45.Howell RW. Auger processes in the 21st century. Int J Radiat Biol. 2008; 84(12): 959-75.
46.Porcel E, Liehn S, Remita H, Usami N, Kobayashi K, Furusawa Y. Platinum nanoparticles: a promising material for future cancer therapy? Nanotechnology. 2010: 21.
47.Paro A, Hossain M, Webster T, Su M. Monte Carlo and analytic simulations in nanoparticle-enhanced radiation therapy. Int J Nanosci. 2016;Volume 11: 4735-4741.
48.Kong T, Zeng J, Wang X, Yang X, Yang J, McQuarrie S, et al. Enhancement of Radiation Cytotoxicity in Breast-Cancer Cells by Localized Attachment of Gold Nanoparticles. Small (Weinheim an der Bergstrasse, Germany). 2008; 4: 1537-1543.
49.Chithrani DB, Jelveh S, Jalali F, van Prooijen M, Allen C, Bristow RG. Gold nanoparticles as radiation sensitizers in cancer therapy. Radiation research. 2010; 173(6): 719-728.
50.Peukert D, Kempson I, Douglass M, Bezak E. Metallic nanoparticle radiosensitisation of ion radiotherapy: A review. Physica Medica. 2018; 47: 121-128.